Pediatr Radiol (2000) 30: 45–51

Joao Ribeiro
Raul C. Ribeiro
Barry D. Fletcher

Imaging findings in pediatric adrenocortical carcinoma

Received: 2 April 1999
Accepted: 5 August 1999

This work was supported in part by the National Cancer Institute, Cancer Center Support (CORE) grant P30 CA21765, and by the American Lebanese Syrian Associated Charities.

J. Ribeiro · R. C. Ribeiro · B. D. Fletcher
International Outreach Program, St. Jude Children's Research Hospital, Memphis, Tennessee, USA

J. Ribeiro
Department of Radiology, Instituto Materno Infantil de Pernambuco, Recife, Brazil

R. C. Ribeiro
Department of Hematology-Oncology, St. Jude Children's Research Hospital, Memphis, Tennessee, USA

R. C. Ribeiro · B. D. Fletcher
Department of Pediatrics, University of Tennessee-Memphis, Tennessee, USA

B. D. Fletcher (✉)
Department of Diagnostic Imaging, St. Jude Children's Research Hospital, 332 N. Lauderdale St., Memphis, TN 38105, USA

B. D. Fletcher
Department of Radiology, University of Tennessee-Memphis, Tennessee, USA
Phone: 901-495-2309; FAX: 901-495-3978; E-mail: barry.fletcher@stjude.org

Abstract *Background.* Adrenocortical carcinoma (ACC), a tumor that is rare among children, causes clinically evident hormonal disturbances. Imaging methods are used to stage disease and to plan surgical resection.
Objective. To describe the findings of the various imaging methods used to evaluate ACC.
Materials and methods. We reviewed the records of ten consecutive patients (mean age, 8.1 years) who presented from 1987 to 1998 with ACC. All patients underwent computed tomography (CT) scanning; five underwent magnetic resonance (MR) imaging; four underwent ultrasonography (US); and eight underwent radionuclide bone scans.
Results. Seven patients presented with signs of hormonally functional tumors. Typical imaging findings consisted of a large, well-defined suprarenal tumor, containing calcifications (seven patients) with a thin capsule and central necrosis or hemorrhage (six patients). The inferior vena cava (IVC) was compressed by tumor in three patients, and ultrasonography demonstrated invasion of the IVC wall in one of these. Three patients' bone scans showed that the primary tumor took up radioactive tracer. Spread to lungs or liver or both was demonstrated in six patients.
Conclusions. CT, US and MR imaging are effective methods of imaging the primary tumor. Chest CT and bone scintigraphy should be performed to detect metastases. The presence of a thin tumor capsule, a stellate central zone of necrosis, and evidence of hormonal function help distinguish ACC from neuroblastoma.

Introduction

Adrenocortical carcinoma (ACC) is a rare tumor, especially among children and adolescents [1, 2]. In these patients, usually girls, the tumors are almost always functional, causing virilization, Cushing's syndrome, or both [1]. Some reports associate the tumor with congenital abnormalities and other tumors [3–5]. The incidence of pediatric ACC appears to be higher in southern Brazil than North America [1]. Abdominal imaging is necessary for detecting ACC and is an important tool for evaluating resectability and planning surgical intervention, because the ability to perform total excision is the most important positive prognostic factor [2]. Previous descriptions of ACC in children have focused on findings from ultrasonography (US) and computed tomography (CT) [6–9]. In this report, we describe our experience with CT scanning, magnetic resonance (MR) imaging, ultrasound (US), and nuclear imaging of children with ACC.

Materials and methods

Ten patients with a diagnosis of ACC proved by histologic findings were treated at our institution between 1987 and 1998. The mean age of the eight girls and two boys was 8.1 years (range 1 to 17 years). Nine patients underwent initial imaging either at the referring institution or in our department at the time of presentation. One patient underwent imaging at the time of recurrence at the primary tumor site. All ten patients underwent CT scanning of the abdomen and thorax, four underwent abdominal US, and five underwent abdominal MR imaging. Radionuclide bone scintigraphy was performed on eight patients, and the skeletal maturation of nine patients was assessed by using radiographs of the hand. All patients underwent unenhanced CT scanning of the chest for the detection of lung metastases. All images were reviewed by two radiologists (J.R., B.D.F.).

The CT scans were evaluated to characterize the following aspects of the primary tumor: size (maximum diameter), definition of tumor margins, calcification, relationship to midline structures, local and regional lymphadenopathy, precontrast attenuation and postcontrast enhancement, presence or absence of a capsule, and inferior vena cava (IVC) involvement. On coronal and transverse MR images, we evaluated the intensity of the tumor on spin-echo T1- and T2-weighted images and (in three patients) on short inversion-time inversion-recovery (STIR) sequences. Contrast-enhancement characteristics (on T1-weighted images) and other variables were also evaluated as on CT scans. On ultrasonographic images, we evaluated IVC involvement. Planar 99m technetium methylene disphosphonate (^{99m} Tc-MDP) bone scans were evaluated for bone metastases and uptake of radioactive tracer by the primary lesion. Bone age was determined for nine patients and was classified as normal or advanced.

Results

Clinical presentation

Six tumors arose in the right adrenal gland and four in the left. Seven tumors were functioning at the time of diagnosis: six patients had signs of virilization, two had associated hypertension, and one had hypertension alone. Bone age was classified as advanced for six patients and as normal for three. Six patients had secondary involvement of the lungs, liver or both. Our series includes one previously reported patient with ACC and a ganglioneuroblastoma that occurred synchronously in the same gland [5]. This patient also had a germline p53 mutation, Turner syndrome, and congenital heart disease consisting of Shone syndrome (coarctation, parachute mitral valve, bicuspid aortic valve) and a ventricular septal defect.

Table 1 Adrenocortical carcinoma: characteristics of the primary tumor (IVC inferior vena cava, ND not done)

Patient	Maximum diameter (cm)	Capsule	Calcification	Central scar	Crossed midline	IVC involvement	Uptake on bone scan
1	10	Yes	Yes	No	No	Not demonstrated	Yes
2	11	Yes	No	Yes	No	Displaced	No
3	16	No	Yes	Yes	No	No	Yes
4	16	No	Yes	Yes	Yes	No	No
5	6.5	Yes	Yes	No	No	No	No
6	4	Yes	No	No	No	No	No
7	2	No	No	No	No	No	No
8	9	No	Yes	Yes	No	Displaced, compressed wall invasion	ND
9	19	Yes	Yes	Yes	Yes	No	ND
10	15	Yes	Yes	Yes	No	Displaced, compressed	Yes

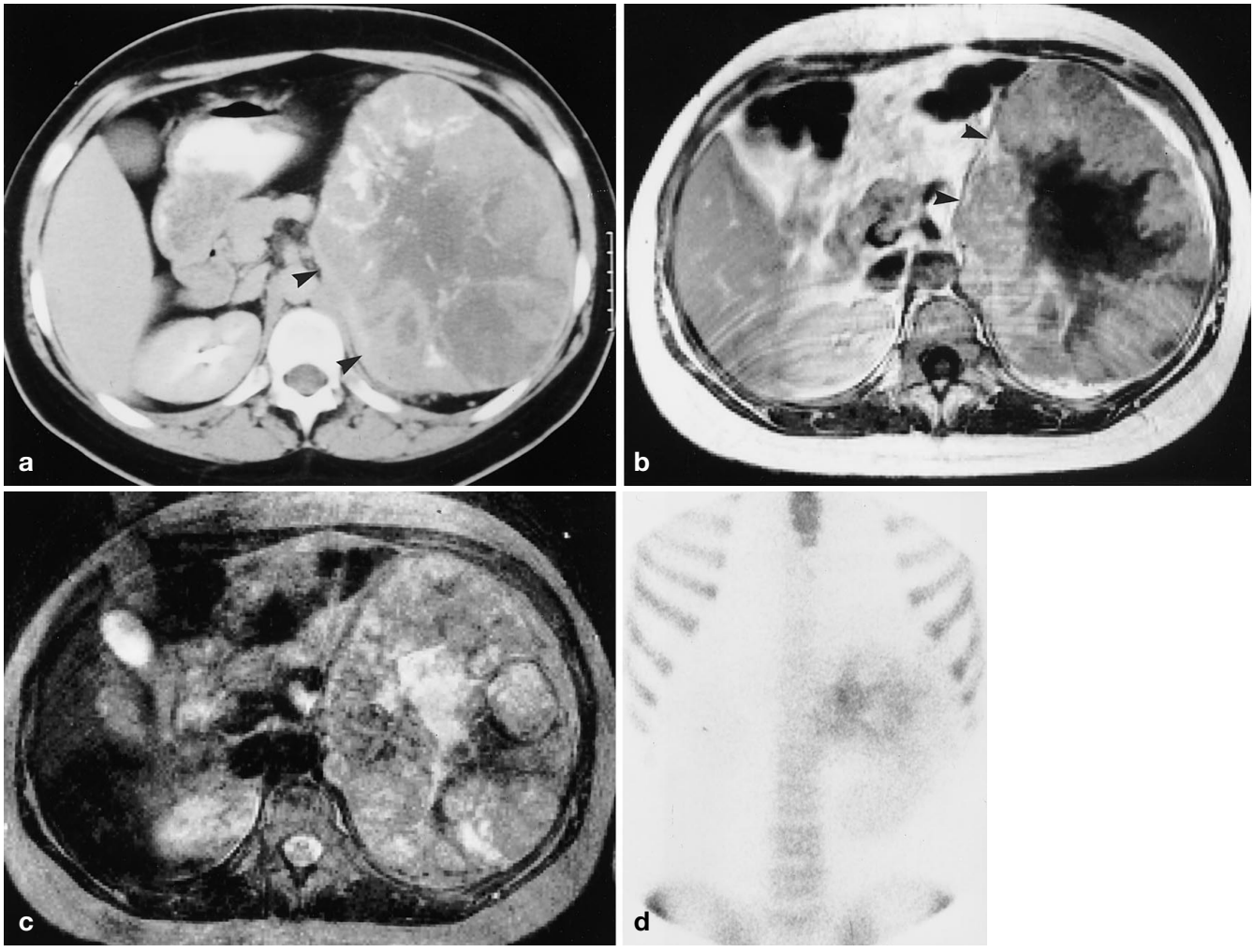

Fig. 1 **a** Contrast-enhanced CT scan of the abdomen shows a well-defined tumor of the left adrenal gland with linear calcifications and enhancement of a thin peripheral capsule *(arrowheads)*. There is a large, irregular central hypoattenuated zone. **b** A contrast-enhanced T1-weighted MR image of the abdomen shows a large hypointense stellate central zone. Note the thin hypointense capsule *(arrowheads)* outlining the medial aspect of the tumor. **c** On T2-weighted MR imaging, the central zone is hyperintense. **d** Planar 99m technetium MDP bone scan: an anterior image of the abdomen shows uptake of radioactive tracer in the left suprarenal mass

Imaging findings

Computed tomography

The tumors ranged in largest diameter from 2 to 19 cm (mean 10.8 cm, Table 1). In nine of the ten patients, the tumor was well defined. In the tenth patient, one of two in whom the tumor had directly invaded the liver, the superior border of the tumor was obscured. Four tumors had no identifiable capsule. The other six tumors were surrounded to some degree by a thin, well-defined enhancing rim. Two of the tumors extended across the midline into the contralateral side of the abdomen. Six tumors contained an irregular area of low attenuation that corresponded to a pathologic finding of necrosis. Calcification, varying from tiny focal deposits to extensive linear and amorphous deposits, was present in seven of the tumors (Figs. 1 a, 2 a).

Two of the four tumors imaged by precontrast CT scanning had a homogeneous appearance, and both enhanced heterogeneously with contrast. On the postcontrast images, nine tumors had a heterogeneous appearance. Only one (the smallest tumor studied) enhanced homogeneously. The patient with this tumor had a second lesion arising from the same adrenal gland. Histologic examination demonstrated that this second lesion was a ganglioneuroblastoma that contained a small calcification (Fig. 3 a). The ACC enhanced less well than the ganglioneuroblastoma.

CT scanning also showed liver metastases in one patient and direct hepatic invasion in two others (Fig. 4 a).

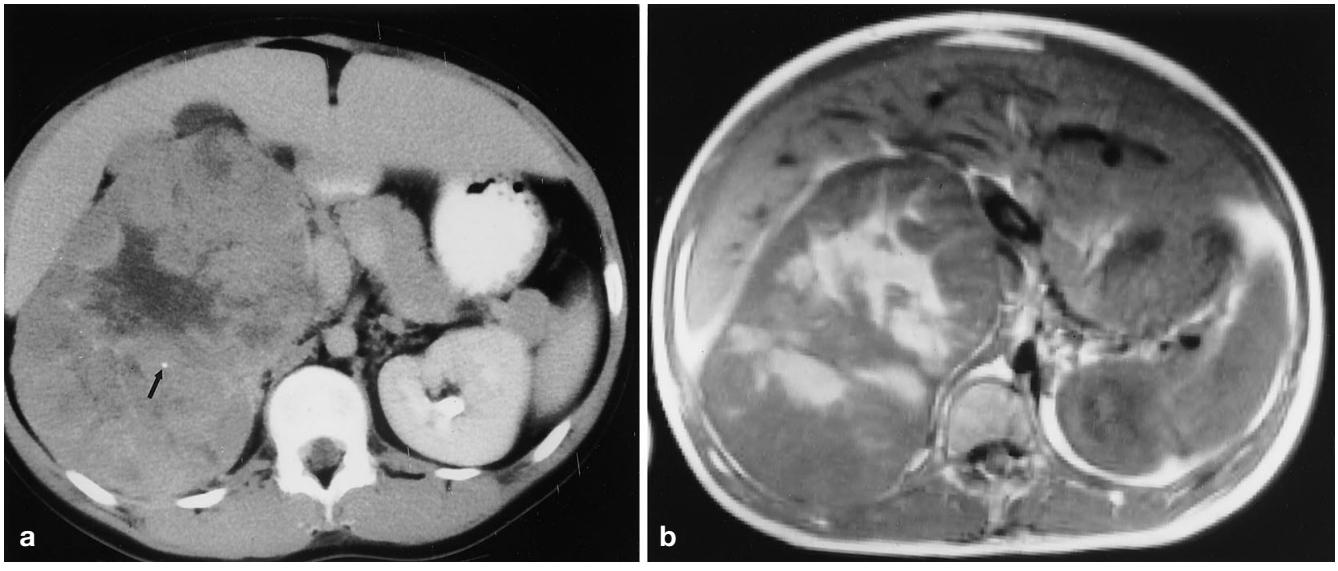

Fig. 2 **a** Contrast-enhanced CT scan of the abdomen shows a large, well-defined right suprarenal mass with a stellate hypoattenuated zone and a tiny calcification *(arrow)*. The tumor extends to the midline and displaces rather than encases large blood vessels such as the inferior vena cava and the aorta. **b** A transverse T1-weighted MR image shows extensive central hyperintensity consistent with hemorrhage within the right suprarenal mass

Fig. 3 **a** Contrast-enhanced CT scan shows two small right suprarenal masses. The larger ACC is less attenuated than the smaller, more medial ganglioneuroblastoma that contains a small calcific focus. **b** A coronal T2-weighted MR image shows the ACC nearly isointense to the kidney and to the visualized portion of the more medial ganglioneuroblastoma. There is a more intense histologically confirmed ACC metastasis at the base of the right lung

These findings were confirmed at surgery in two of these three patients. In all of these patients, the ACC arose from the right adrenal gland. Three patients had lung metastases, two had liver involvement alone, and one had both lung and liver metastases. One of the patients with lung metastases had a hyperattenuated nodule in the subcutaneous fat of the anterior abdominal wall, but its cause was not pathologically confirmed.

We could not identify local or regional abdominal lymph-node enlargement as distinct from the primary tumor in any of the patients. Imaging did not detect retrocrural or distant lymphadenopathy in any patient. The IVC was displaced anteromedially in three patients, all with tumors of the right adrenal gland. In two patients, the IVC was also compressed, and in one there was also anterior displacement and slight compression of the portal vein. In one patient, the IVC was not well demonstrated. In the remaining seven, it was well demonstrated without signs of invasion or compression.

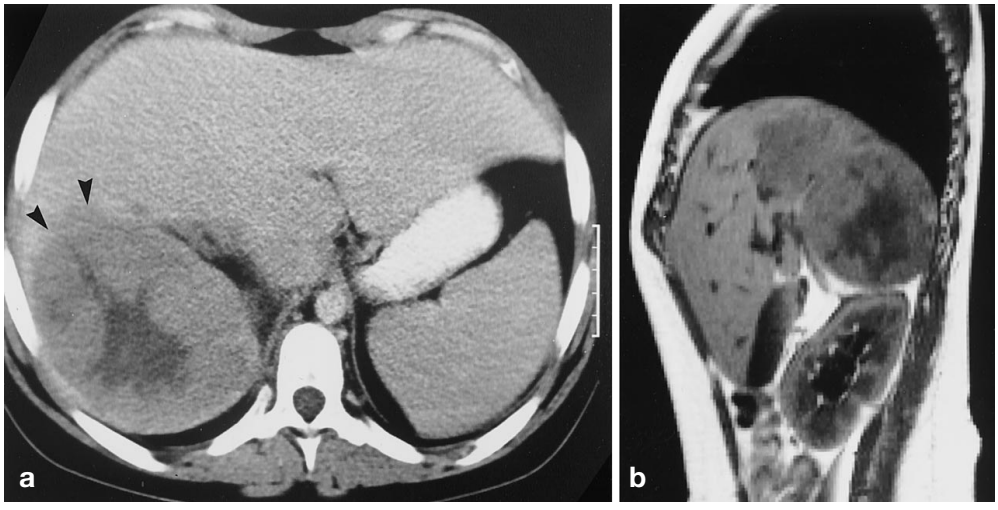

Fig. 4 **a** Contrast-enhanced CT scan shows poor definition of the anterolateral margin of a right suprarenal ACC *(arrowheads)* due to surgically proven extension into the liver. **b** A sagittal T1-weighted MR image of the abdomen shows involvement of the posterior aspect of the right lobe of the liver by the adjacent ACC. Note the hypointense central zone

Displacement and mild compression of the ipsilateral kidney occurred with the larger tumors, but in no case was there renal invasion.

Magnetic resonance imaging

Five patients underwent MR imaging of the abdomen. In four, the tumor was isointense to muscle on T1-weighted images; in one, the mass was hyperintense. On T2-weighted images, the mass was isointense to hyperintense as compared to subcutaneous fat in two patients, hyperintense in two, and isointense in one patient. STIR sequences were performed on three patients, and in all three the tumor was isointense as compared to water. In the patient with both ACC and ganglioneuroblastoma, the ACC was slightly more intense than the ganglioneuroblastoma on T1-weighted images and was of similar intensity on T2-weighted images (Fig. 3 b).

The mass was well defined in all five patients who underwent MR imaging. In the patient with liver invasion, sagittal images complemented CT in localizing the intrahepatic portion of the tumor (Fig. 4 b). In all five patients, a thin hypointense tumor capsule surrounding part or all of the tumor was visible on noncontrasted T1- and T2-weighted images (Fig. 1 b, c).

Intensity of all tumors except one was heterogeneous on precontrast T1-weighted images. The three tumors imaged with contrast agent showed heterogeneous enhancement. Two tumors exhibited a hypointense nonenhancing central area corresponding to the hypoattenuated area seen on CT images (Fig. 1 b). This feature was similar in appearance to the "central scar" described in liver tumors [10] (Table 1); it became hyperintense in comparison with fat on T2-weighted images (Fig. 1 c) and was also hyperintese on STIR images. The central zone of one other tumor was hyperintense on the unenhanced T1-weighted images, possibly because of hemorrhagic content, and its intensity did not change with the administration of IV contrast agent (Fig. 2 b).

Evaluation of lymph nodes and kidneys by MR imaging showed no intrinsic renal abnormalities and no lymphadenopathy. The IVC was well shown in four patients by both MR imaging and CT scanning, but in one the MR image showed anterior compression by the tumor that was not demonstrated by CT scanning. In the two patients with IVC compression, a slight intraluminal signal visible on T1-weighted images was interpreted as the result of slow velocity. In one patient, the intrahepatic portion of the IVC could not be visualized by either imaging method.

Ultrasonography

For the four patients who underwent US, the examination was performed primarily to evaluate the IVC. In two patients, IVC compression was demonstrated, and in one patient, involvement of the IVC wall was demonstrated by US but not by CT scanning or MR imaging (Fig. 5). The IVC of one patient appeared to be normal. Patency of the IVC was well demonstrated in all cases by Doppler flow imaging. The central zones in three tumors demonstrated by CT scanning and MR appeared hypoechoic on ultrasonographic images.

Bone scan

The findings of bone scintigrams were negative for bone metastases in all eight patients who underwent scintigraphy. In three, the tumor took up the radioactive tracer (Fig. 1 d); all of these tumors had calcifications that

were visible on CT scans. Two calcified tumors lacked avidity for the radiotracer.

Discussion

In patients with ACC, both CT scanning and MR imaging readily show the primary tumor. On CT scans, ACC typically appears as a well-defined, partially calcified tumor with a thin, enhancing peripheral capsule and an irregular hypoattenuated nonenhancing central area. The central area, which resembles the central scar seen in primary liver tumors [10], was found in six of the ten tumors in our series. On CT scans, it appears as an irregular hypoattenuated area [9] and on ultrasonographic images as a hypoechoic zone [7]. In our series, it was also visible on T1-weighted MR imaging as a hypointense, or in one instance hyperintense, region that did not enhance. On T2-weighted and STIR images, the central scar was hyperintense. In the case of ACC, this central area correlates with confluent necrosis, hemorrhage, or fibrosis [6, 9, 11].

ACC spreads locally to liver, lymph nodes, the diaphragm, and the renal vein. IVC invasion is uncommon, but can occur with tumors of either the left or the right adrenal gland [12]. Compression of the IVC by the tumor can also result in thrombosis [9]. If the tumor extends to the right atrium, cardiopulmonary bypass may be necessary to accomplish complete tumor excision. Because right atrial extension may be missed on CT scans [12], US and possibly MR imaging should be performed.

In our patients, metastases occurred only in the liver and lungs. One patient had both liver and lung metastases. Interestingly, the tumors of all of the patients with liver involvement were located in the right adrenal gland, a finding previously reported [13]. Lymph-node involvement was not identified in this study. No bone metastases were detected in the eight patients who underwent ^{99m}Tc-MDP bone scintigrams.

Most malignant tumors arising from the adrenal gland during childhood are neuroblastomas or ganglioneuroblastomas. Other less common suprarenal masses include cysts, adenomas, pheochromocytomas myelolipomas, and metastases [8, 9]. In the absence of metasta-

Fig. 5 **a** Contrast-enhanced CT shows a partially calcified right suprarenal tumor with paracaval extension. The inferior vena cava *(arrow)* is displaced but appears patent. **b** A transverse ultrasonographic image through the upper abdomen shows compression of the inferior vena cava by the suprarenal mass. **c** Apparent invasion of the wall of the inferior vena cava is demonstrated on a longitudinal ultrasonographic image. The tumor was dissected away from the vein wall at surgery

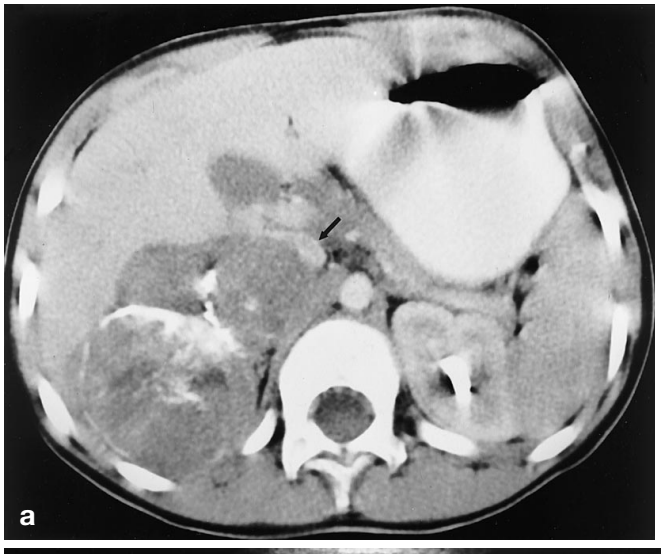

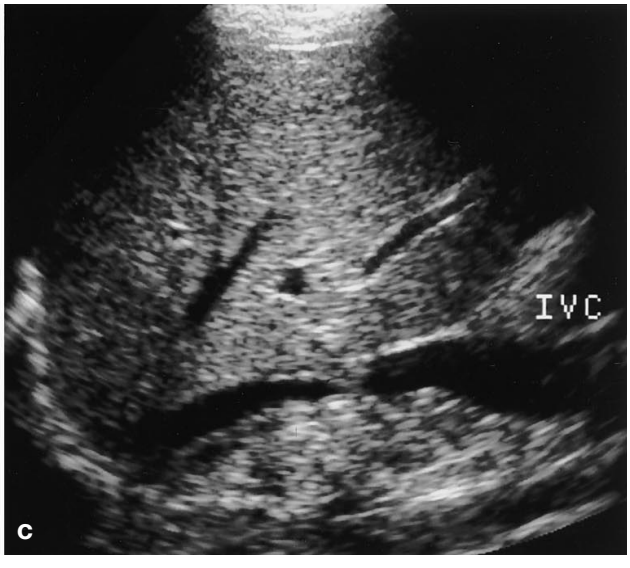

ses, ACC cannot be reliably differentiated from adrenal adenoma on clinical or pathological grounds [14]. Although large size (> 6 cm) and heterogeneity of the tumor at imaging suggests malignancy, one of the malignant tumors in this series that presented with metastases was only 2 cm in diameter. The demonstration of fat within the adrenal tumors on MR images has been reported to be a reliable indicator of adenoma, but lipid-sensitive phase-selective sequences have also demonstrated fat in adrenocortical carcinoma [15]. Agrons et al. [14] have proposed that the inclusive term "adrenocortical neoplasm" be applied to these tumors in childhood.

Neuroblastomas occur in younger patients; 75 % are less than 4 years of age [16]. Although adrenal neuroblastomas infrequently exhibit hormonal activity, they cannot usually be differentiated from ACC by imaging methods alone. At the time of diagnosis, both types of tumors tend to be large and to have areas of calcification and necrosis; the pattern of calcification is variable but frequently ringlike [16, 17]. We found primarily dense calcifications in our study, but there were some instances of ringlike and mottled calcifications.

An imaging feature that may aid in distinguishing ACC from neuroblastoma is the presence of a central stellate zone. Although necrosis is common in neuroblastoma [16], it does not usually assume the stellate appearance that characterized the central zone of the ACC tumors in our patients. In one of our patients, the zone was hyperintense on both T1- and T2-weighted MR imaging, a finding consistent with hemorrhage. A thin enhancing rim on CT scan may also be a specific finding in ACC [11], but it was not present in any of our cases.

Uptake of the radioactive tracer by the tumor was demonstrated on three of the eight ^{99m} Tc-MDP bone scintigrams. This phenomenon can also occur in nearly 75 % of neuroblastomas [18]. Therefore, the presence or absence of primary tumor uptake cannot be used as a differential diagnostic feature. In our series, both of the tumors that took up ^{99m} Tc-MDP were calcified. However, in neuroblastoma, no association between calcification and primary tumor uptake has been established [18].

In our study, three patients had metastases in the lungs, a rare event in neuroblastoma, and none of our patients had bone metastases detected by scintigraphy; such metastases are common for patients with neuroblastoma.

In summary, CT scanning, US, and MR imaging are effective methods of imaging ACC. CT scanning of the chest is necessary for detecting pulmonary metastases, which are frequently associated with ACC. US or MR imaging should be performed to detect invasion or thrombosis of the inferior vena cava. Radionuclide bone scintigraphy is used to evaluate skeletal metastases and, as is the case with neuroblastoma, may show uptake of radioactive tracer by the primary tumor. A diagnosis of ACC rather than neuroblastoma should be considered if the tumor contains a central stellate zone of apparent necrosis and displaces or invades major adjacent blood vessels such as the IVC. However, the correct diagnosis of ACC is more often based on clinical and laboratory findings rather than imaging because most of these tumors are hormonally functional in the pediatric population.

References

1. Sandrini R, Ribeiro RC, DeLacerda L (1997) Extensive personal experience. Childhood adrenocortical tumors. J Clin Endocr Metab 82: 2027–2031
2. Ribeiro RC, Sandrini R, Schell MJ, et al (1990) Adrenocortical carcinoma in children: a study of 40 cases. J Clin Oncol 8: 67–74
3. Levine GW (1978) Adrenocortical carcinoma in two children with subsequent primary tumors. Am J Dis Child 132: 238–240
4. Lee PD, Winter RJ, Green OC (1985) Virilizing adrenocortical tumors in childhood: eight cases and review of the literature. Pediatrics 76: 437–443
5. Pivnick EK, Furman WL, Velagaleti GVN, et al (1998) Simultaneous adrenocortical carcinoma and ganglioneuroblastoma in a child with Turner syndrome and germline p53 mutation. J Med Genet 35: 328–332
6. Prando A, Wallace S, Marins JLC, et al (1990) Sonographic findings of adrenal cortical carcinomas in children. Pediatr Radiol 20: 163–165
7. Hamper UM, Fishman EK, Hartman DS, et al (1987) Primary adrenocortical carcinoma: sonographic evaluation with clinical and pathologic correlation in 26 patients. AJR 148: 915–919
8. Daneman A, Chan HSL, Martin J (1983) Adrenal carcinoma and adenoma in children: a review of 17 patients. Pediatr Radiol 13: 11–18
9. Dunnick NR, Heaston D, Halvorsen R, et al (1982) CT appearance of adrenal cortical carcinoma. J Comput Assist Tomogr 6: 978–982
10. Rummeny E, Weissleder R, Sironi S, et al (1989) Central scars in primary liver tumors: MR features, specificity, and pathologic correlation. Radiology 171: 323–326
11. Fishman EK, Deutch BM, Hartman DS, et al (1987) Primary adrenocortical carcinoma: CT evaluation with clinical correlation. AJR 148: 531–535
12. Godine LB, Berdon WE, Brasch RC, Leonidas JC (1990) Adrenocortical carcinoma with extension into inferior vena cava and right atrium: report of 3 cases in children. Pediatr Radiol 20: 166–169
13. Castleman B, Scully RE, McNeely BU (1972) Case records of the Massachusetts General Hospital: case 46–1972. N Engl J Med 287: 1033–1040
14. Agrons GA, Lonergan GJ, Dickey GE, et al (1999) Adrenocortical neoplasms in children: radiologic-pathologic correlation. Radiographics 19: 989–1008
15. Schlund JF, Kenney PJ, Brown ED, et al (1995) Adrenocortical carcinoma: MR imaging appearance with current techniques. J Magn Reson Imaging 5: 171–174
16. Bousvaros A, Kirks DR, Grossman H (1986) Imaging of neuroblastoma: an overview. Pediatr Radiol 16: 89–106
17. Araki T, Itai Y, Iio M (1982) CT features of calcification in abdominal neuroblastoma. J Comput Assist Tomogr 6: 789–791
18. Podrasky AE, Stark DD, Hattner RS, et al (1983) Radionuclide bone scanning in neuroblastoma: skeletal metastases and primary tumor localization of 99mTc-MDP. AJR 141: 469–472